ChemComm

Accepted Manuscript

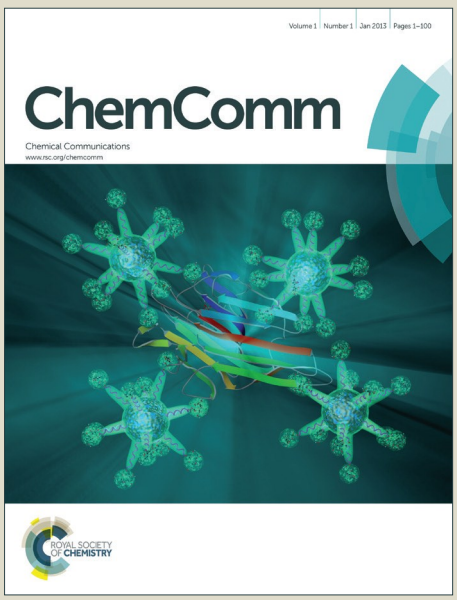

ROYAL SOCIETY OF CHEMISTRY

www.rsc.org/chemcomm

Journal Name

RSCPublishing

COMMUNICATION

One Versatile Spatially Confined Self-assembly Strategy to Construct Multifunctional Metal Oxide@ Cyanometallate-based Coordination Polymer Heterostrutures

Cite this: DOI: 10.1039/x0xx00000x

Received 00th January 2012,
Accepted 00th January 2012

DOI: 10.1039/x0xx00000x

www.rsc.org/

Fan-Xing Bu,[a] Li Xu,[a] Wei Zhang,[a] Chuan-Yin Jin,[a] Rui-Juan Qi,[b] Rong Huang[b] and Ji-Sen Jiang*[a]

We developed one versatile spatially confined self-assembly strategy to integrate cyanometallate-based coordination polymers with functional metal oxides into well-defined core@shell heterostructures. The structure, composition, size and morphology of the heterostructures could be facilely controlled. The obtained Fe_3O_4@Prussian blue heterostructure has been evaluated as an appealing multifunctional thermal ablation agent exhibiting response to both magnetic field and light irradiation.

Prussian blue (PB) and related cyanometallate-based coordination polymers (CMCPs), as one kind of classical coordination polymers consisting of metal ions coordinated by CN bridges, have attracted extensive attention due to their excellent performance in many potential applications such as molecular magnets, catalysts, biomedical materials and secondary batteries.[1] Recently, there has been a growing interest in modifying the properties of CMCPs or endowing them multifunctionality by tailoring the architecture of CMCPs and constructing CMCPs based heterostructures.[2] Among them, integrating CMCPs with non-CMCPs functional materials (NCFMs) has been demonstrated as an effective route.[3] For example, grafting PB nanoparticles on multi-walled carbon nanotubes improves the electrocatalytic activity towards H_2O_2 reduction.[3a] Coating gold nanoparticles with Prussian blue analogue (PBA) combines the plasmonic optical properties of the gold core and the magnetic properties of the PBA shell.[3b] Intercalating PB into titania nanosheet ultrathin films creates photomagnetic materials.[3c] These kinds of CMCPs based heterostructures have wide application prospects, for they not only feature a simple combination of the physical and chemical properties of CMCPs with NCFMs but also often display novel properties that originate from the mutual interactions between them. Thus it is highly desirable to construct novel and featured multifunctional materials by combining CMCPs and various NCFMs both with unique properties, and explore their potential applications.

To realize the successful integration of CMCPs with NCFMs, the nucleation and growth of CMCPs has to be confined on the surface of NCFMs. However, CMCPs are often obtained by precipitation reaction between metal ions and cyanometallate ions. The reaction is too fast to be easily controlled in homogeneous solutions, not to speak of confining the reaction on the surface of NCFMs, thus special measurements have been adopted. The first available route is adsorption-induced nucleation and super-slow growth mediated by super-slow simultaneous addition of metal ions and cyanometallate ions into the same solutions containing NCFMs.[3b] And the second one is adsorption-induced nucleation and step-by-step assembly by dispersing NCFMs alternately in solutions containing metal ions and cyanometallate ions.[3c] These methods are impressive and could be used to fabricate other heterostructures materials where their shells suffer from similar problems.[4] Nevertheless, the complex and

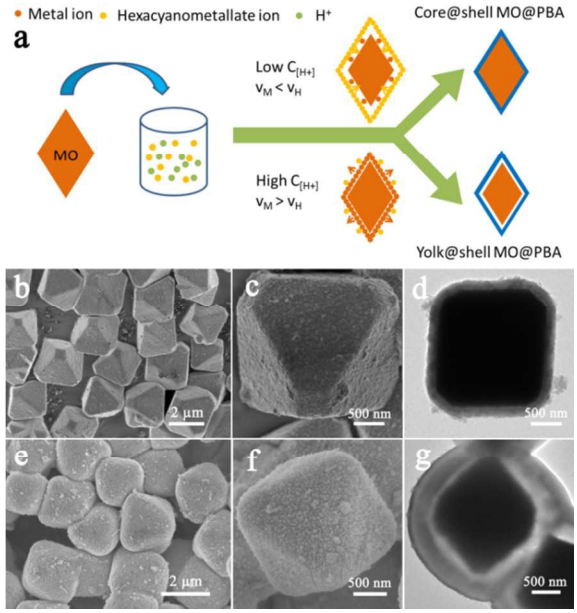

Fig. 1 (a) Schematic illustration of the formation of MO@CMCP heterostructure by spatially confined self-assembly method. (MO: metal oxide; CMCP: cyanometallate-based coordination polymer; $C_{[H+]}$: concentration of H^+; V_M , V_C: diffusion rate of metal ions and cyanometallate ions). (b,e) Low magnified FESEM, (c,f) high magnified FESEM and (d,g) TEM images of core@shell structured and yolk@shell structured Cu_2O@Cu-Fe PBA heterostructures, respectively.

tedious synthetic procedures impose huge obstacles to the construction of CMCPs based heterostructures and further exploration of their promising properties. Therefore, a new facile and versatile strategy is urgently needed.

Here, we present one novel and simple spatially confined self-assembly strategy to integrate CMCPs with NCFMs into well-defined core@shell heterostructures by using metal oxides (MOs) as the model NCFMs. The strategy is designed based on the simultaneous dissolution of MOs and the formation of CMCPs on the surface of MOs, which resolve the problem that CMCPs were not easy to nucleate and grow on the surface of MOs by simple one-pot process. MOs are chosen as the typical NCFMs to demonstrate our concept owing to three points. Firstly, MOs can be considered as the presentative NCFMs that could dissolve in acidic solution to supply metal ions for the formation of CMCPs and thus the reaction kinetic can be easily and finely controlled. Secondly, MOs can be integrated with other NCFMs into well-defined core@shell structure,[5] which holds tremendous possibility for the integration of those NCFMs that cannot provide dissolved metal ions with CMCPs. Thirdly, MOs have excellent optical, magnetic and electrochemical properties that often possessed by CMCPs, and it is highly possible that the heterostructures of CMCPs and MOs would exhibit combined, synergetic and even coupled properties. Remarkably, this strategy is so versatile that the structure, composition, size and morphology of the MO@CMCP heterostructures could be mediated simply by controlling the nature of MOs and cyanometallate ions and the acidity of reaction solution. Quite encouragingly, the obtained Fe_3O_4@PB heterostructure has been evaluated as an appealing multifunctional thermal ablation agent exhibiting response to both magnetic field and light irradiation firstly.

In a typical procedure, MOs were dispersed into water solution containing cyanometallate ions and reaction would be initiated by the introduction of acid. Here, metal ions would be controllably released from the surface of MOs by acidic etching and be confined on the surface of MOs by reacting with cyanometallate ion. At the same time, the MOs also acted as substrates to support the growth and self-assembly of CMCPs to form a layer of robust shell. It is to be noted that the convection diffusion that the released metal ions diffused from the surface of MOs to the solution while cyanometallate ions diffused from the solution to the surface of MOs proceed around the MOs framwork. By controlling the acidity, the dissolution rate of MOs could be easily tailored to regulate the diffusion rate of metal ions. At low H^+ concentration, the diffusion rate of cyanometallate ions is larger than metal ions, core@shell structured MO@CMCP would be formed, otherwise, yolk@shell structured MO@CMCP would be created as schematically shown in Fig. 1a.

Semiconductors Cu_2O and copper ferrocyanide (Cu-Fe PBA) were chosen as typical core and shell to demonstrate our envision at first, for Cu_2O is of diverse non-spherical morphology and often was used as sacrificial template to fabricate hollow-structured materials due to their weak stability in concrete environment.[6] As shown in field emission scanning electron microscope (FESEM) image (Fig. 1b and 1c), the obtained products followed a typical procedure in relatively low [H^+] by using slightly truncated octahedral Cu_2O as core are well-dispersed uniform truncated octahedral particles with uneven surface consisting of large amount of intergrown nanocubes, which are quietly different from pristine Cu_2O with smooth exterior (Fig. S1). The obvious contrast difference between the centre and edge region of one particle in transmission electron microscope (TEM) image (Fig.1d) revealed that the obtained product was core@shell heterostructure, which could be further confirmed by the different elemental distribution of Fe from Cu in elemental mapping images of one particle (Fig. S2a). Stronger Cu signal was detected at the centre than the edge of one particle due to much higher Cu content in the core than the shell. However, Fe tended to uniformly distribute across the whole particle because they only existed in the shell. In addition, the existence of K was confirmed by elemental analysis based on energy dispersive X-ray (EDX) analysis (Fig. 2Sb), which is a common phenomenon.[1f, 1g] X-ray diffraction (XRD) pictures in Fig. S2c showed that the peaks of shell could be well-assigned to face centered cubic lattice Cu-Fe PBA (JCPDS card 86-0514). The adsorption peaks at 2086 cm^{-1} and 493 cm^{-1} attributed to CN stretching and Fe^{II}-CN-Cu^{II} in Fourier-transform infrared (FT-IR) spectrum (Fig. S2d) further confirmed its composition.[7] These results demonstrated that core@shell structured Cu_2O@Cu-Fe PBA heterostructure was successfully obtained by this spatially confined self-assembly method.

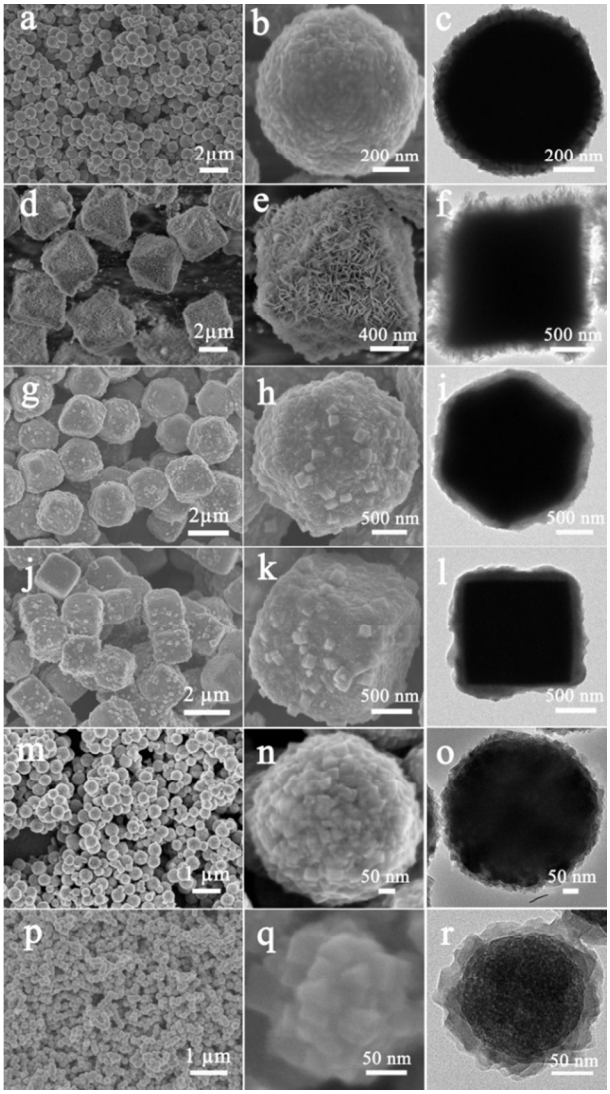

Fig. 2 Low magnified FESEM, high magnified FESEM and TEM images of core@shell structured Fe_3O_4@PB heterostructure (a-c), Cu_2O@Cu-Ni CP heterostructure (d-f), Cu_2O@Cu-Fe PBA heterostructures (g-i, j-l) obtained by using Cu_2O with different morphology (cubooctahedron, truncated cube) and Fe_3O_4@PB heterostructures (m-o, p-r) obtained by using Fe_3O_4 with different size (430 nm, 170 nm), respectively.

When the acidity of the reaction system was increased to certain value, the dissolution rate of Cu_2O would be largely accelerated and yolk@shell other than core@shell structured Cu_2O@Cu-Fe PBA

heterostructure (Fig. 1e-g and Fig. S3) appeared. As displayed in Fig. 1e and 1f, the prepared products are uniform octahedrons with rounded corners and edges, and the nanoparticle building blocks that construct their surface are smaller than those of the above core@shell heterostructure (Fig. 1c). These differences were mainly caused by the faster dissolution rate of Cu_2O and crystallization rate of Cu-Fe PBA. TEM picture and elemental mapping for Cu and Fe of one particle (Fig. 1g and S3a) completely confirmed that yolk@shell heterostructure was created. EDX, XRD and FT-IR analysis (Fig. S3b-d) demonstrated that the shell is face centered cubic structured Cu-Fe PBA (JCPDS card 86-0514). That is to say, the structure of Cu_2O@Cu-Fe PBA could be facilely controlled by changing acidity of the solution in this spatially confined self-assembly method. It can be reasonably speculated that the cyanometallate ions are just like hunters, waiting for capturing metal ions once they appeared. When the the amount of metal ions is modest, the hunters could terminate them at the moment they are released, leading to core@shell Cu_2O@Cu-Fe PBA heterostructures. While large amount of metal ions are released, the hunters would be retarded at the surface of the Cu_2O and yolk@shell Cu_2O@Cu-Fe PBA heterostructure would be obtained. This acidity-controllable structure transformation process is a very feasible and interesting process, providing us an insight into the effective structural control of the heterostructure in this diffusion controlled reaction system.

As one new kind of interesting and meaningful strategy to integrate MOs and CMCPs, the universality of this method for synthesizing other heterostructures with different compositional MOs and CMCPs is of crucial importance. By using core@shell structure as model, we change the composition of MOs and CMCPs to demonstrate the facility of our work. Appropriately choosing the species and concentration of the used acid based on the nature of MOs and CMCPs is the key of this reaction system. And the facility to vary this critical factor becomes its great advantages compared to other systems.[8] Firstly, Cu_2O was substituted to Fe_3O_4 with strong acidic stability. By utilizing HCl as H^+ source, core@shell structured Fe_3O_4@PB was successfully fabricated. Fig. 2a and 2b displayed that the obtained Fe_3O_4@PB heterostructure well-inherited the spherical architecture of Fe_3O_4 (Fig.S4) and had rough surfaces that composed by intergrown PB nanocubes. TEM picture and elemental mapping for Fe and K of one particle (Fig. 2c and S5a) affirmed its core@shell structure. Elemental and crystal structural analysis (Fig. S5b-d) demonstrated that the coordination polymer shell is face centered cubic PB (JCPDS card 01-0239).[9] Then, the attempt to obtain CMCP shell with non-cubic structure was also carried out. By replacing potassium ferricyanide with potassium tetracyanonickelate and using Cu_2O octahedron as core (Fig. S6), hierarchical core@shell Cu_2O@$[Cu(H_2O)_2Ni(CN)_4]$[10] (Cu-Ni CP) heterostructure (Fig. 2d-f and Fig. S7) with two dimentional Cu-Ni CP flakes intergrown on the Cu_2O was easily prepared.

Engineering the size and morphology of material, especially with core@shell structure[11] is an attractive and effective route to adjust their properties. Thus it is appealing to obtain size- and morphology-controllable core@shell structured MO@CMCPs heterostructures. These factors were also examined in this paper to further demonstrate the versatility of our work. Considering the convenience to change the morphology of Cu_2O and to vary the size of spherical Fe_3O_4, we try to obtain morphology-controllable Cu_2O@Cu-Fe PBA heterostructures and size-controllable Fe_3O_4@PB heterostructures. Firstly, the morphology of Cu_2O was varied from truncated octahedron (Fig. S1) to cubooctahedron (Fig. S8) and then truncated cube (Fig. S9). Irrelevant to their different morphology, conformal coating of Cu-Fe PBA on Cu_2O cores was realized as shown in Fig.2g-l and Fig. S10, S11. They are all Cu_2O@Cu-Fe PBA heterostructures with their shells built from intergrown Cu-Fe PBA nanocubes. Then the size of Fe_3O_4 was changed from 750 nm (Fig. S4) to 430 nm (Fig. S12) and 170 nm (Fig. S13), and we obtained core@shell structured Fe_3O_4@PB heterostructures resoundingly as shown in Fig. 2m-r and Fig. S14, S15. In a word, this spatially confined self-assembly strategy is very versatile and it has little limitation to the composition, structure, size and morphology of the core and shell, which holds great potential for its wide application.

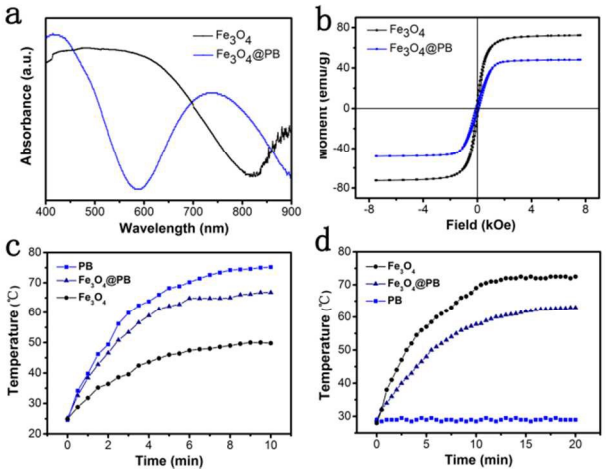

Fig. 3 (a) UV−vis absorption spectra and (b) Magnetization curves of the Fe_3O_4 particles with size about 170 nm and corresponding core@shell structured Fe_3O_4@PB heterostructure; Temperature change of Fe_3O_4@PB heterostructure, Fe_3O_4 particles and PB particles dispersion under NIR laser irradiation for 10 min (c) and under magnetic field for 20 min (d).

Considering the ideal integration of MOs and CMCPs, the core@shell structured Fe_3O_4@PB heterostructure obtained by using Fe_3O_4 particles with size about 170 nm was used as model material to evaluate the multifunctionality of the obtained heterostructures by this versatile method, for Fe_3O_4 and PB are all important and well-recognized biomedical materials.[1c-e, 12] When Fe_3O_4@PB was examined as hyperthermia agent, they not only exhibited response to magnetic field but also NIR laser irradiation. As shown in Fig. 3a and 3b, the as-synthesized Fe_3O_4@PB heterostructure exhibited a typical absorption peak of PB around 750 nm compared to original Fe_3O_4 particles and reasonable saturation magnetization of about 48 emu•g^{-1} derived from original Fe_3O_4 particles. As the heterostructure was exposed to an 808 nm laser with an output power of 2 W, the temperature of the solution rose to 66.2 °C from 23 °C after 10 min (Fig. 3c). Simultaneously, at a magnetic field of 34.8 kA m^{-1}, the temperature of the magnetic heterostructure solution increased to 63 °C from 29 °C within 20 min (Fig. 3d). The photothermal and magnetothermal effect of original Fe_3O_4 particles and PB particles obtained by removing Fe_3O_4 from the heterostructure were both carried out for comparison. Obviously, PB particles have outstanding photothermal effect while Fe3O4 particles have prominent magnetothermal effect, and the combination of them endows the Fe3O4@PB heterostructure both quite excellent photothermal and magnetothermal effect. What is more, the Fe_3O_4@PB heterostructure exhibits excellent photothermal and magnetothermal stability, and no obvious temperature loss was observed in the following two cycles (Fig. S16). This result indicates that this heterostructure combines the optical properties of the PB shell and the magnetic properties of the Fe_3O_4 core and can be used as potential multiple-responses thermal ablation agent for cancer therapy. That is to say, we could obtain multifunctional heterostructures by using this spatially confined self-assembly method to integrate components with different properties together.

Conclusions

In conclusion, we have developed a novel and versatile spatially confined self-assembly strategy to fabricate well-dispersed core@shell and yolk@shell structured MO@CMCP heterostructures in a controllable way. This strategy is based on simultaneous dissolution of MOs and formation of CMCPs due to their different stability in acidic solution. Not only is this strategy applicable to MOs and CMCPs with various components, but also allows facile engineering of the size and morphology of the resulted heterostructures by varying the size and morphology of MOs. Moreover, the typical Fe_3O_4@PB heterostructure has been performed as thermal ablation agent exhibiting response to both magnetic field and light irradiation, demonstrating the MO@CMCP heterostructures are potential multifunctional platforms. More promisingly, the successful integration of CMCPs with MOs into core@shell heterostructures may provide unprecedented opportunities for the design of NCFM@CMCP heterostructures with more complex compositions and structures. The present work makes a significant contribution to the synthetic methodology of NCFM@CMCP heterostructures and may pave the way for the future exploration of the properties of these heterostructures.

Acknowledgments

This work was supported by the National Natural Science Foundation of China (Grant Nos. 21473059, 21173084) and Large Instruments Open Foundation of East China Normal University.

Notes and references

[a] Department of Physics, Center for Functional Nanomateriels and Devices, East China Normal University, Shanghai 200241, P.R. China.
[b] Key Laboratory of Polar Materials and Devices, Ministry of Education, East China Normal University, Shanghai 200241, P.R. China.
E-mail: jsjiang@phy.ecnu.edu.cn

Electronic Supplementary Information (ESI) available: Detailed experimental procedures. FESEM and XRD pictures of Cu_2O and Fe_3O_4. TEM, elemental mapping, EDX, XRD and FT-IR analysis of Cu_2O@Cu-Fe PBA heterostructures, Cu_2O@Cu-Ni CP heterostructure and Fe_3O_4@PB heterostructures. The cyclic performance of the Fe_3O_4@PB heterostructure for (a) photothermal and (b) magnetothemal effect. See DOI: 10.1039/c000000x/

1 (a) H. Tokoro and S. Ohkoshi, *Dalton Trans*, 2011, **40**, 6825; (b) F. X. Bu, M. Hu, L. Xu, Q. Meng, G. Y. Mao, D. M. Jiang and J. S. Jiang, *Chem. Commun.*, 2014, **50**, 8543; (c) G. Fu, W. Liu, S. Feng and X. Yue, *Chem. Commun.*, 2012, **48**, 11567; (d) M. Shokouhimehr, E. S. Soehnlen, J. Hao, M. Griswold, C. Flask, X. Fan, J. P. Basilion, S. Basu and S. D. Huang, *J. Mater. Chem.*, 2010, **20**, 5251; (e) X. Liang, Z. Deng, L. Jing, X. Li, Z. Dai, C. Li and M. Huang, *Chem. Commun.*, 2013, **49**, 11029; (f) C. D. Wessells, R. A. Huggins and Y. Cui, *Nat Commun*, 2011, **2**, 550; (g) Y. You, X. L. Wu, Y. X. Yin and Y. G. Guo, *Energy Environ. Sci*., 2014, **7**, 1643.

2 (a) M. Hu, S. Furukawa, R. Ohtani, H. Sukegawa, Y. Nemoto, J. Reboul, S. Kitagawa and Y. Yamauchi, *Angew. Chem. Int. Ed.*, 2012, **51**, 984; (b) M. Hu, A. A. Belik, M. Imura and Y. Yamauchi, *J . Am. Chem. Soc.*, 2012, **135**, 384; (c) M. Hu, N. L. Torad and Y. Yamauchi, *Eur. J. Inorg. Chem.*, 2012, **30**, 4795; (e) C. R. Gros, M. K. Peprah, B. D. Hosterman, T. V. Brinzari, P. A. Quintero, M. Sendova, M. W. Meisel and D. R. Talham, *J . Am. Chem. Soc.*, 2014, **136**, 9846; (g) D. Asakura, C. H. Li, Y. Mizuno, M. Okubo, H. Zhou and D. R. Talham, *J . Am. Chem. Soc.*, 2013, **135**, 2793;

3 (a) J. Li, J. D. Qiu, J. J. Xu, H. Y. Chen and X. H. Xia, *Adv. Funct. Mater.*, 2007, **17**, 1574; (b) G. Maurin-Pasturel, J. Long, Y. Guari, F. Godiard, M. G. Willinger, C. Guerin and J. Larionova, *Angew. Chem. Int. Ed.*, 2014, **53**, 3872; (c) T. Yamamoto, N. Saso, Y. Umemura and Y. Einaga, *J . Am. Chem. Soc.*, 2009, **131**, 13196.

4 (a) F. Ke, L. G. Qiu, Y. P. Yuan, X. Jiang and J. F. Zhu, *J. Mater. Chem.*, 2012, **22**, 9497; (b) M. E. Silvestre, M. Franzreb, P. G. Weidler, O. Shekhah and C. Wöll, *Adv. Funct. Mater.*, 2013, **23**, 1210.

5 (a) H. Sun, J. He, J. Wang, S. Y. Zhang, C. Liu, T. Sritharan, S. Mhaisalkar, M. Y. Han, D. Wang and H. Chen, *J . Am. Chem. Soc.*, 2013, **135**, 9099; (b) Y. Zhang, H. Ding, Y. Liu, S. Pan, Y. Luo and G. Li, *J. Mater. Chem.*, 2012, **22**, 10779; (c) C. H. Kuo, T. E. Hua and M. H. Huang, *J . Am. Chem. Soc.*, 2009, **131**, 17871.

6 (a) D. F. Zhang, H. Zhang, L. Guo, K. Zheng, X. D. Han and Z. Zhang, *J. Mater. Chem.*, 2009, **19**, 5220; (b) Z. Wang, D. Luan, F. Y. C. Boey and X. W. Lou, *J . Am. Chem. Soc.*, 2011, **133**, 4738; (c) J. Nai, Y. Tian, X. Guan and L. Guo, *J . Am. Chem. Soc.*, 2013, **135**, 16082; (d) C. H. Kuo, Y. Tang, L. Y. Chou, B. T. Sneed, C. N. Brodsky, Z. Zhao and C. K. Tsung, *J . Am. Chem. Soc.*, 2012, **134**, 14345.

7 (a) C. Loos-Neskovic, S. Ayrault, V. Badillo, B. Jimenez, E. Garnier, M. Fedoroff, D. J. Jones and B. Merinov, *J. Solid State Chem.*, 2004, **177**, 1817; (b) M. Avila, L. Reguera, J. Rodríguez-Hernández, J. Balmaseda and E. Reguera, *J. Solid State Chem.*, 2008, **181**, 2899.

8 (a) W. W. Zhan, Q. Kuang, J. Z. Zhou, X. J. Kong, Z. X. Xie and L. S. Zheng, *J . Am. Chem. Soc.*, 2013, **135**, 1926; (b) J. Reboul, S. Furukawa, N. Horike, M. Tsotsalas, K. Hirai, H. Uehara, M. Kondo, N. Louvain, O. Sakata and S. Kitagawa, *Nature Mater.*, 2012, **11**, 717; (c) K. Khaletskaya, J. Reboul, M. Meilikhov, M. Nakahama, S. Diring, M. Tsujimoto, S. Isoda, F. Kim, K. i. Kamei, R. A. Fischer, S. Kitagawa and S. Furukawa, *J . Am. Chem. Soc.*, 2013, **135**, 10998.

9 (a) L. Lin, X. Huang, L. Wang and A. Tang, *Solid State Sci.*, 2010, **12**, 1764; (b) F. X. Bu, C. J. Du, Q. H. Zhang and J. S. Jiang, *CrystEngComm*, 2014, **16**, 3113.

10 (a) Y. Mathey and C. Mazieres, *Can. J. Chem.*, 1974, **52**, 3637; (b) J. Rodríguez-Hernández, A. A. Lemus-Santana, C. N. Vargas and E. Reguera, *C. R. Chimie*, 2012, **15**, 350.

11 (a) B. Zhang, D. Wang, Y. Hou, S. Yang, X. H. Yang, J. H. Zhong, J. Liu, H. F. Wang, P. Hu, H. J. Zhao and H. G. Yang, *Sci. Rep.*, 2013, **3**; (b) H. Ataee-Esfahani, J. Liu, M. Hu, N. Miyamoto, S. Tominaka, K. C. W. Wu and Y. Yamauchi, *Small*, 2013, **9**, 1047; (c) Y. Rui, Y. Li, Q. Zhang and H. Wang, *Nanoscale*, 2013, **5**, 12574; (d) J. Liu, S. Z. Qiao, J. S. Chen, X. W. Lou, X. Xing and G. Q. Lu, *Chem. Commun.*, 2011, **47**, 12578; (e) T. Yang, R. Zhou, D. W. Wang, S. P. Jiang, Y. Yamauchi, S. Z. Qiao, M. J. Monteiro and J. Liu, *Chem. Commun.*, 2015, **51**, 2518; (f) T. Yang, J. Liu, R. Zhou, Z. Chen, H. Xu, S. Z. Qiao and M. J. Monteiro, *J. Mater. Chem. A*, 2014, **2**, 18139.

12 G. Y. Mao, W. J. Yang, F. X. Bu, D. M. Jiang, Z. J. Zhao, Q. H. Zhang, Q. C. Fang and J. S. Jiang, *J. Mater. Chem. B*, 2014, **2**, 4481.

